(p,n) Reactions in ^{48}Ca, ^{90}Zr, ^{120}Sn, and ^{208}Pb

R. R. Doering, Aaron Galonsky, and D. M. Patterson

A. Quasi-Elastic Scattering, a Macroscopic Global Analysis.

A global, energy-dependent, Lane-model, nucleon-nucleus optical potential has been determined by fitting (p,n)-IAS angular distributions between 25 and 45 MeV while maintaining the fit obtained by Becchetti and Greenlees[1] (BG) to proton elastic-scattering data. Differential cross sections for transitions to the isobaric analogs of the target ground states have been extracted from neutron time-of-flight spectra such as the example in Fig. 1.

In the Lane model,[2] the optical potential is

$$U=-U_o+4U_1(\underset{\sim}{t}\cdot\underset{\sim}{T})/A,$$

where $\underset{\sim}{t}$ and $\underset{\sim}{T}$ are the nucleon and nucleus isospins, respectively, and A is the mass number of the nucleus. We wish to parameterize U with a linear energy dependence. As there are two characteristic energies involved in the (p,n)-IAS reaction, due to the non-zero Q-value, it is not entirely clear what energy should be used in the parameterization. As suggested by George Bertsch, we choose

$$U(r,k)=U_C(r)+1/2[U_E(r)K+KU_E(r)],$$

where K is the kinetic-energy operator. To simplify the use of the potential, we replace K by an appropriate average value, giving

$$U(r,E)=-U_{OC}-U_{OE}E+4[U_{1C}+U_{1E}E](\underset{\sim}{t}\cdot\underset{\sim}{T})/A,$$

where $E=E_p-\bar{V}_c$ for the p-target system, $E_p-\Delta_c$ for the n-analog system, $1/2(2E_p-\bar{V}_c-\Delta_c)$ for the (p,n)-IAS form factor, and E_n for the n-target system.

In order to reduce the number of free parameters, we use the BG Coulomb-corrected proton potential (BGVC) to specify U_{OC} and U_{OE}. The geometry for each U_1 term is chosen to be the same as for the corresponding U_0 term. It is further assumed that U_1 can be specified by a real volume term plus an imaginary surface term. Thus, there are four free parameters: the strengths of the volume and surface parts of U_{1C} and of U_{1E}.

Values for these parameters have been determined by using a non-linear least-squares search program with the DWBA program DWUCK as the function subroutine. Global searches have been performed using all of our (p,n)-IAS data. As the potential is parameterized directly in terms of U_0 and U_1, Lane-model consistency is automatically maintained; i.e., the proton and neutron potentials used to generate the distorted waves change as U_1 is varied. Since it is necessary to maintain the fit to the proton elastic-scattering data obtained by BG while improving the fit to our (p,n)-IAS data by adjusting U_1, we correct U_0 for changes in U_1. Our parameters generate proton elastic-scattering cross sections which are almost the same as those obtained by BG.

Figure 2 shows our (p,n)-IAS data along with the results of DWBA calculations using isovector strengths U_{1C}=17.7 MeV, U_{1E}=0 for the real volume well and U_{1C}=18.1 MeV, U_{1E}=-0.31 for the imaginary surface well (solid lines). The dashed lines in Fig. 2 are obtained by using the BGVC proton parameters, the BG "Common" neutron parameters, and the (p,n) form-factor prescription of Hoffmann.[3,4] Our fits are clearly as good as, or better than, those obtained with the BGVC parameters.

If the Lane model is valid, the potentials resulting from our searches should be able to predict neutron elastic-scattering cross sections. Figure 3 shows the predictions (solid lines). The targets selected are all those for which there are (n,n) data from 7 to 24 MeV.[5] The dashed lines in Fig. 3 are obtained with the BG "Common" neutron parameters.[1] Our parameters reproduce the data as well as, if not better than, the BG parameters. While previous attempts to use (p,n)-IAS data and the Lane model to determine neutron optical parameters have been successful for single energies and for individual targets, our parameters reproduce neutron elastic-scattering data over a large range of neutron energy and target mass, even though most of the targets are different from those included in the (p,n)-IAS data used to determine the parameters.

B. (p,n)-IAS Transitions, a Microscopic Description.

The central-force part of the effective nucleon-nucleon interaction may be expressed in the form:

$$V_{ij}=V_0g_0(r_{ij})+V_\sigma g_\sigma(r_{ij})\underset{\sim}{\sigma}_i\cdot\underset{\sim}{\sigma}_j+V_\tau g_\tau(r_{ij})\underset{\sim}{\tau}_i\cdot\underset{\sim}{\tau}_j+V_{\sigma\tau}g_{\sigma\tau}(r_{ij})\underset{\sim}{\sigma}_i\cdot\underset{\sim}{\sigma}_j\underset{\sim}{\tau}_i\underset{\sim}{\tau}_j.$$

Since the isospin-flip term of the effective interaction is the only central-force component which contributes to the direct amplitude for charge-exchange scattering to $J^\pi=0^+$ isobaric analog states (IAS), these reactions are quite sensitive to V_τ.

The measured and theoretical angular distributions are given in Fig. 4. The principal error in absolute magnitude of the data is an estimated ±10% for neutron detection efficiency calculations.[6] Theoretical angular distributions in Fig. 4 have been calculated with the code DWBA,[7] which includes the "knockon" exchange amplitude without approximations. The proton

and neutron distorted waves have been generated with BGVC optical-model parameters.[1] For ^{120}Sn the bound states have been represented by BCS wave functions.[8] Elementary shell-model configurations in Woods-Saxon potentials have been assumed for the other targets: $(f_{7/2})^8$, $0.8(g_{9/2})^{10} + 0.6(g_{9/2})^8(p_{1/2})^2$, and $(h_{9/2})^{10}(f_{7/2})^8(i_{13/2})^{14}(p_{3/2})^4(f_{5/2})^6(p_{1/2})^2$ for the excess neutrons in ^{48}Ca, ^{90}Zr, and ^{208}Pb, respectively. The dashed curves result from phenomenological nucleon-nucleon forces[9] with V_τ=12 MeV (short dashes) and with V_τ=18 MeV (long dashes). The solid curves have been calculated with a realistic force derived by Bertsch[10] from the central, even part of the Reid soft-core potential.[11]

Both the phenomenological and realistic forces yield angular distributions which follow the data but are generally smoother. The similarity in shape of the dashed and solid curves results from the $0^+ \rightarrow 0^+$ IAS transitions being dominated by the monopole component of $V_\tau g_\tau(r_{ij})$. With the 1.0-F range Yukawa form for g_τ, the best overall fits to our data at proton energies of 25, 35, and 45 MeV are obtained with V_τ=19 1/2, 15 1/2, and 13 1/2 MeV, respectively. The G-matrix interaction produces nearly the same cross sections for these reactions as a 1.0-F Yukawa with V_τ=13 1/2 MeV. Thus, it accounts for the data quite well at 45 MeV and fairly well at 35 MeV. However, the experimental cross sections at 25 MeV are consistently larger than predicted.

Additional estimates of V_τ may be obtained from optical-model analyses of elastic and "quasi-elastic" (charge-exchange) scattering. To first order in the effective nucleon-nucleon interaction, V_τ is proportional to the magnitude of the real isovector term in the optical-model potential.[12] A macroscopic DWBA analysis of 94-MeV (p,n)-IAS data[13] yields only about 1/3 the isospin-flip strength found in a similar study at 40 MeV.[14] Satchler has suggested[15] that the large energy dependence may only reflect uncertainties in the optical-model parameters available for DWBA calculations at 94 MeV. Nevertheless, using the parameters quoted by Thurlow,[13] we have been able to fit the 94-MeV data for ^{27}Al, ^{51}V, and ^{208}Pb with V_τ averaging 8 1/2 MeV, a decrease of only 37% from our value at 45 MeV. The apparent discrepancy between the macroscopic and microscopic analyses results from the very limited angular range of the 94-MeV data coupled with the sensitivity of the forward-angle peak to the form-factor. Thus, more extensive angular distributions are necessary for a reliable determination of V_τ at 94 MeV.

It has been suggested that neutron pickup followed by proton stripping may interfere with the direct amplitude.[16] The significance of (p,d)(d,n) contributions is currently under investigation by several groups including our own. However, we have demonstrated that straightforward DWBA calculations employing reasonable forces are capable of accounting for (p,n)-IAS angular distributions to a degree comparable with analogous (p,p') data.

C. Excited Analog States, Isovector Deformation

The (p,n) reaction to an analog state has been called quasi-elastic scattering, i.e. elastic scattering with a charge exchange. In quasi inelastic scattering the analog of an excited state of the target is produced.[17] Just as (p,p) and (p,n) to the IAS of the target ground state determine U_0 and U_1, the spherical isoscalar and isovector parts of the optical potential, (p,p') and (p,n) to the excited analog state (EAS) determine β_0 and β_1, the isoscalar and isovector deformation parameters of the potential. The analogs of 2^+ states in ^{26}Mg and ^{56}Fe are strongly excited at 18 MeV and require the two-step amplitudes $0^+ \rightarrow 2^+$(p,p') followed by $2^+ \rightarrow 2^+$ quasi-elastic scattering and $0^+ \rightarrow 0^+$ quasi-elastic scattering followed by $0^+ \rightarrow 2^+$(n,n').[18] Because the one- and two-step amplitudes had a relative phase of ~90°, the calculation was unfortunately insensitive to the value of β_1. In our (p,n) spectra excited analog states are either not seen or are much smaller than ground state IAS. A spectrum in which two EAS are relatively prominent is shown in Fig. 5. We have such data for targets of ^{90}Zr and ^{120}Sn with E_p=25, 35, and 45 MeV. With both 2^+ and 3^- data we may be able to determine both the quadrupole and octupole deformations of the isovector part of the potential. It would be interesting to compare these with the corresponding isoscalar deformations.

D. Pre-Equilibrium Neutrons

In addition to the sharp structure of analog states in our neutron spectra there is a continuum of pre-equilibrium neutrons. When an excited compound nucleus exists, neutrons are emitted in familiar fashion from a state of statistical equilibrium, i.e., they are evaporated. Since nuclear temperatures are only ~1 MeV, evaporation is negligible in producing neutrons above 5-10 MeV. Other processes, currently under study, are responsible. These processes occur in the early stages of the proton-nucleus interaction, when the incident kinetic energy has had time to be shared with only a few nucleons. It is during this period, long before equilibrium has been achieved that high-energy nucleons are emitted with relatively high probability. Spectra

resulting from bombardment with 45-MeV protons are shown in Fig. 6. Each spectrum is the angular integral of 32 differential spectra obtained at neutron emission angles from 0° to 160°. The target thicknesses are 11, 100, 86, and 232 keV for ^{48}Ca, ^{90}Zr, ^{120}Sn, and ^{208}Pb, respectively. For 25- and 35 MeV proton bombardment we have similar data. We are collaborating with Professor M. Blann of the University of Rochester in investigating the detailed pre-equilibrium mechanism[19] by which these high-energy neutrons are produced.

REFERENCES

1. F. D. Becchetti, Jr. and G. W. Greenlees, Phys. Rev. 182, 1190(1969).
2. A. M. Lane, Phys. Rev. Lett. 8, 171(1962) and Nucl. Phys. 35, 676(1962).
3. G. W. Hoffmann, Phys. Rev. C8, 761(1973).
4. P. D. Kunz, L. D. Rickertsen, and G. W. Hoffmann, Phys. Rev. C9, 1659(1974).
5. Data obtained from Angular Distributions in Neutron Induced Reactions (BNL 400), National Neutron Cross Section Center, Brookhaven National Laboratory, Upton, New York (1970).
6. R. Kurz, University of California Report UCRL-11399 (1964), unpublished; S. T. Thornton and J. R. Smith, Nucl. Instr. and Meth. 96, 551(1971).
7. R. Schaeffer and J. Raynal, Distorted-wave-Born-approximation code, Center for Nuclear Studies of Saclay (1970), unpublished.
8. Vincent Gillet, Bertrand Giraud, and Mannque Rho, Nucl. Phys. A103, 257(1967).
9. Sam M. Austin, "The Effective Two-Nucleon Interaction from Inelastic Proton Scattering," in The Two-Body Force in Nuclei, ed. by S. M. Austin and G. M. Crawley (New York, Plenum Press, 1972), 285.
10. G. Bertsch, The Practitioner's Shell Model (Amsterdam, North-Holland Publishing Co., 1972), 79.
11. R. Reid, Ann. Phys. 50, 411(1968).
12. P. E. Hodgson, Nuclear Reactions and Nuclear Structure (Oxford, Claredon Press, 1971), Chap. 6; D. Slanina and H. McManus, Nucl. Phys. A116, 271(1968).
13. Nola Thurlow, Nucl. Phys. A109, 471(1968).
14. R. K. Jolly, T. M. Amos, A. Galonsky, R. Hinrichs, and R. St Onge, Phys. Rev. C7, 1903(1973).
15. G. R. Satchler, "Isospin Dependence of Optical Model Potentials", In Isospin in Nuclear Physics, ed. by D. W. Wilkinson (Amsterdam, North-Holland Publishing Co., 1969), 391.
16. L. D. Rickertsen and P. D. Kunz, Phys. Lett. 47B, 11(1973).
17. G. R. Satchler, R. M. Drisko, and R. H. Bassel, Phys. Rev. 136, B637(1964).
18. V. A. Madsen, M. J. Stomp, V. R. Brown, J. D. Anderon, Luisa Hansen, Calvin Wong, and J. J. Wesolowski, Phys. Rev. Lett. 28, 629(1972).
19. M. Blann, Nucl. Phys. A213, 570(1973).

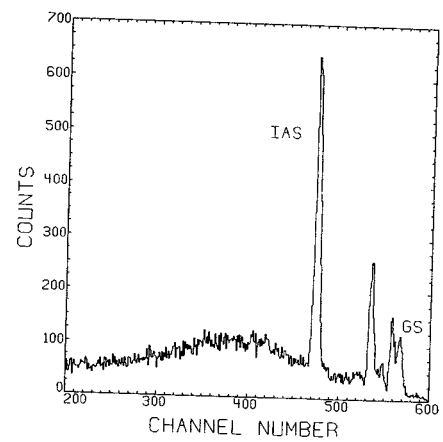

Fig. 1.--Neutron time-of-flight spectrum for $^{90}Zr(p,n)^{90}Nb$ at E_p=35 MeV. The scattering angle is 0° and the flight path is 7.22 m.

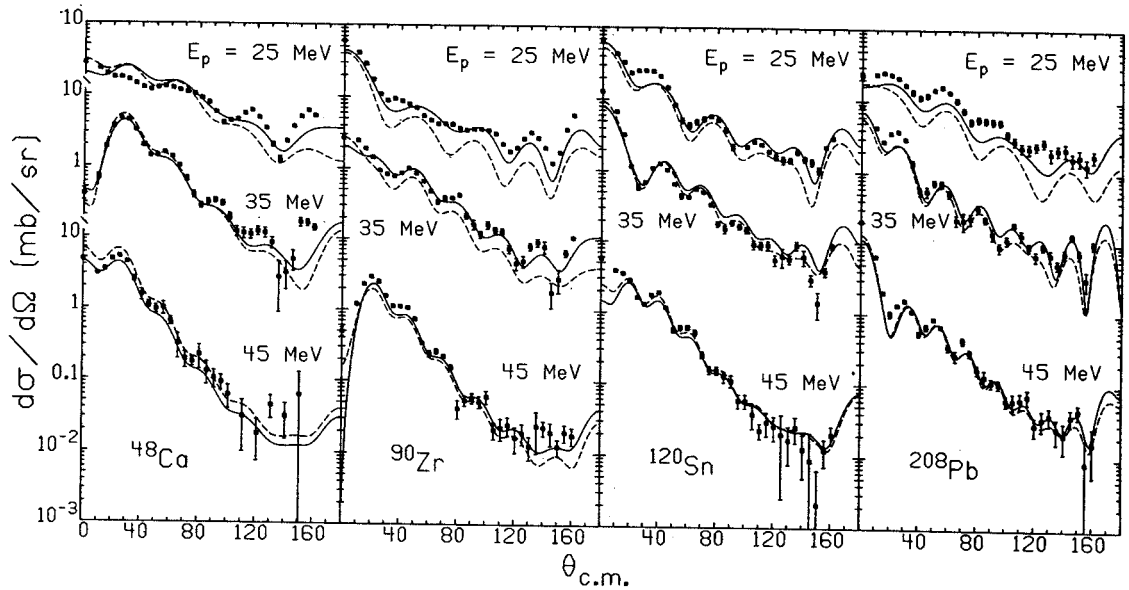

Fig. 2.--Comparisons of DWBA calculations with (p,n)-IAS differential cross-section data. The solid curves were obtained with our parameters, the dashed curves with those of Becchetti and Greenlees.

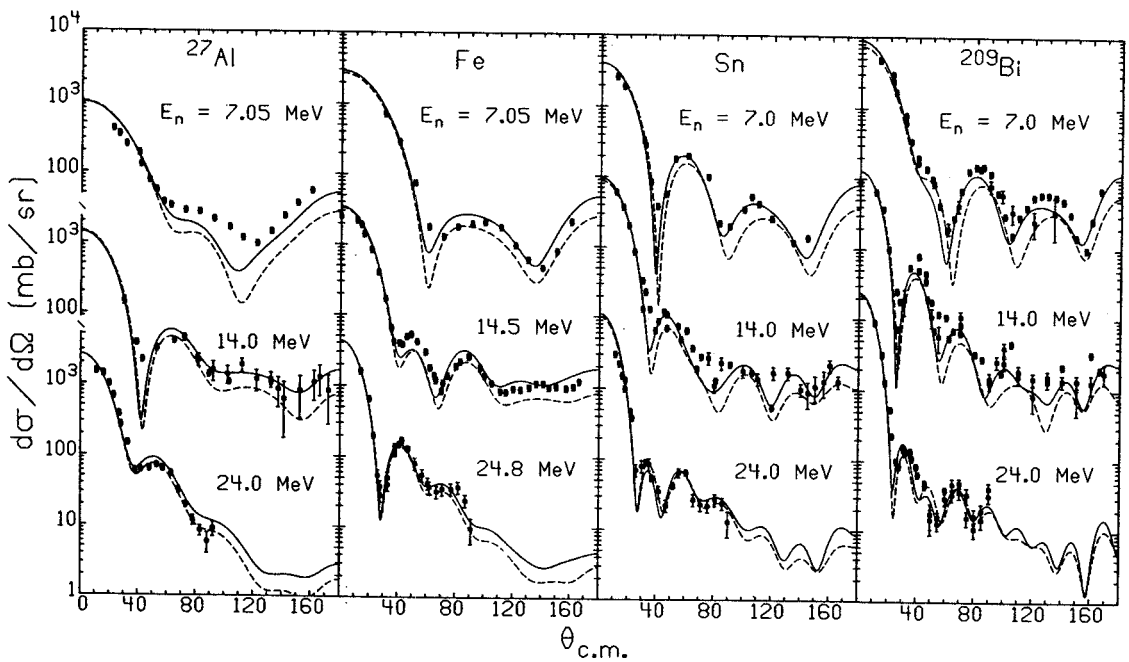

Fig. 3.--Comparisons of optical-model calculations with (n,n) elastic differential cross-section data. The solid curves were obtained with our parameters, the dashed curves with those of Becchetti and Greenlees.

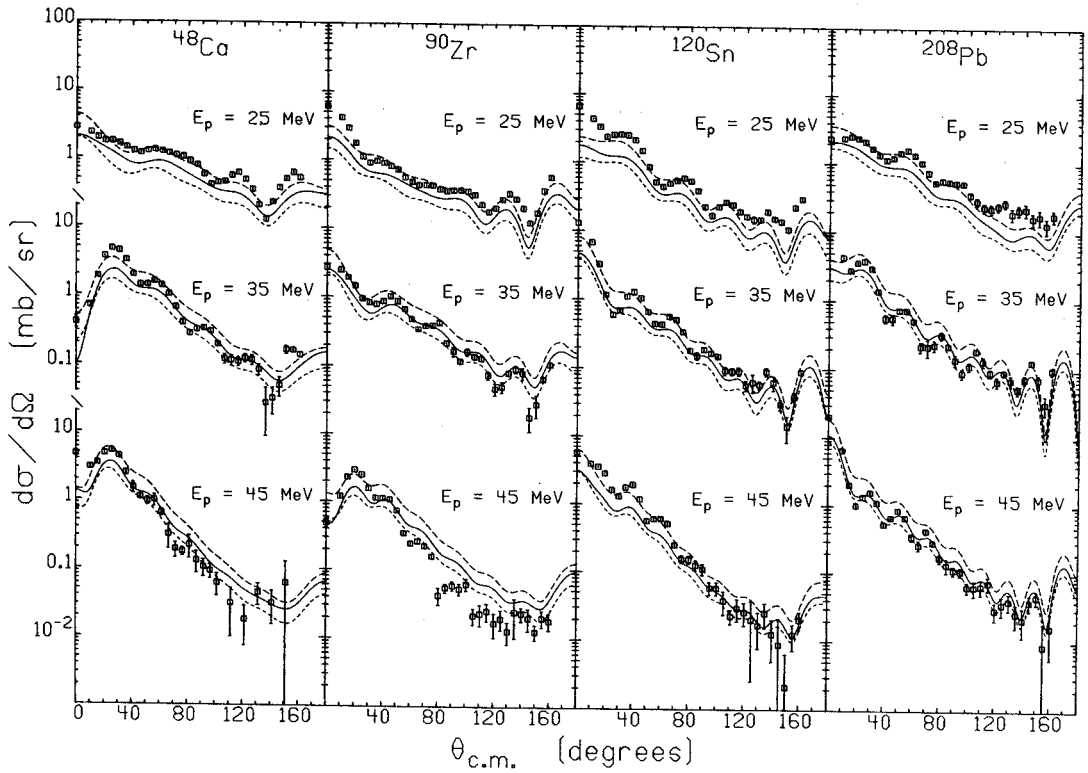

Fig. 4.--Comparison of experimental (p,n)-IAS angular distributions with microscopic DWBA calculations based on phenomenological (dashed) and G-matrix (solid) effective nucleon-nucleon interactions. The short and long dashes correspond to V_τ=12 and 18 MeV, respectively.

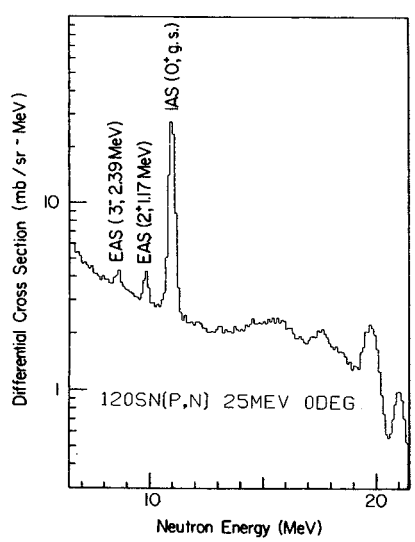

Fig. 5.--(p,n) spectrum showing analogs of the ground state of ^{120}Sn and of its collective 2^+ and 3^- excited states.

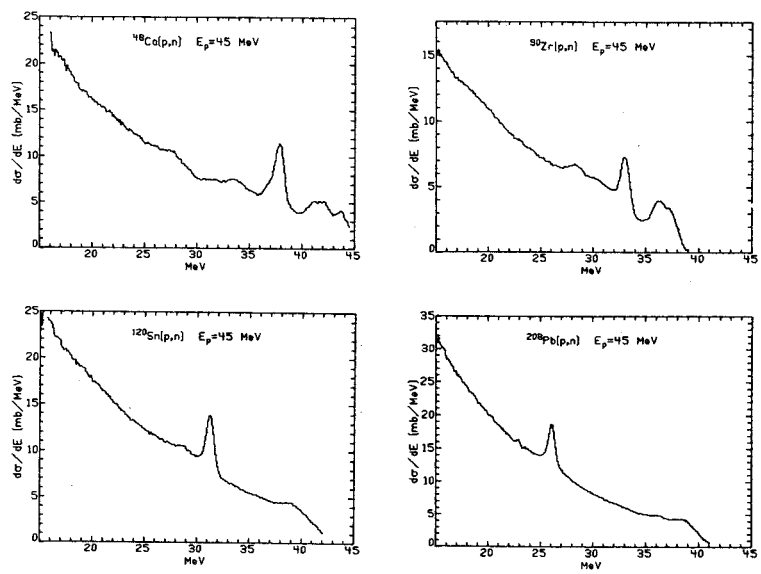

Fig. 6.--Angle-integrated cross sections for neutron production vs. neutron energy.

$^{14}C(p,n)$ Reaction and the Tensor Force

Mike Cabot, Sam M. Austin, R. R. Doering, Aaron Galonsky, and D. M. Patterson

From the time that the quadrupole moment of the deuteron was measured, it has been known that a component of the nuclear interaction is the tensor force, but it has been difficult to obtain an accurate and consistent picture of its importance. In 1957 it was shown by Visscher and Ferrell[1] that the tensor force was essential for an explanation of the anomalously long beta-decay lifetime of ^{14}C. Although a super-allowed pure Gamow-Teller ($0^+ \rightarrow 1^+$) transition, the lifetime is four orders of magnitude greater than simple $(p_{1/2})^2$ wave functions would predict. By constructing wave functions of both $p_{1/2}$ and $p_{3/2}$ orbitals and including a tensor two-nucleon interaction Visscher and Ferrell were able to explain the inhibition via cancellation of terms in the beta-decay matrix element. No mixture of purely central forces is capable of giving the required cancellation. Hence the long lifetime of ^{14}C is a boon not only to archaeology, but also to nuclear physics.

The $^{14}C(p,n)$ reaction to the ground state of ^{14}N negotiates a transition between the same nuclear states as in ^{14}C beta decay. The ordinarily-dominant L=0 contribution to this charge-exchange reaction is very nearly proportional to the allowed beta-decay matrix element, which is fortuitously suppressed. The tensor interaction, which is spin dependent and mixes an L=0 transfer to the nucleon with an L=2 transfer to the nucleus, may predominate over, or at least be comparable to, the central forces. A detailed experimental and theoretical study of this reaction has been made at energies up to 18 MeV.[2] Inconsistent results, however, were obtained between differential cross sections, which clearly favored inclusion of a tensor force, and neutron polarization measurements, which did not. Deficiencies in this work are: (1) neglect of knock-on exchange amplitude, (2) neglect of compound-nucleus effects, and (3) inability to fit the $0^+ \rightarrow 0^+$ (2.31 MeV) IAS transition, presumably because of difficulties with the optical model; these difficulties are also present in analysis of the ground-state transition in which the tensor force is present.

We are in the midst of calculating and measuring $^{14}C(p,n)$ cross sections between 25 and 45 MeV. Our computer program, DWBA-70, includes knock-on exchange. In the 25-45 MeV range compound nucleus effects should be quite negligible and the DWBA should be very applicable. With all these advantages that come with higher energy also come the experimental difficulties of smaller cross sections and faster neutrons to resolve. By developing an epoxy bonding scheme[3] we have produced a target with 3.5 mg/cm^2 of ^{14}C to counteract the low cross sections; short cyclotron bursts and a good detector have enabled us to achieve sufficient energy resolution. Some data have been taken at 25, 35, and 45 MeV. A typical spectrum at 25 MeV, θ_n=60°, is shown in Figure 1. Transitions to the three lowest states of ^{14}N are of interest. The IAS transition to the 2.31 MeV state is governed mostly by the distorted waves and by V_τ, the isospin-flipping part of the central force. Transitions to the 1^+, T=0 states at 0 and 3.95 MeV are governed by the same (almost) distorted waves; by $V_{\sigma\tau}$, the spin- and isospin-flipping part of the central force; and by the tensor force.

REFERENCES

1. W. M. Visscher and R. A. Ferrell, Phys. Rev. 107, 781(1957).

2. C. Wong, J. D. Anderson, V. A. Madsen, F. A. Schmittroth, and M. J. Stomp, Phys. Rev. C3, 1904(1971).

3. M. Cabot, et al., to be published in Nucl. Instr. and Methods.

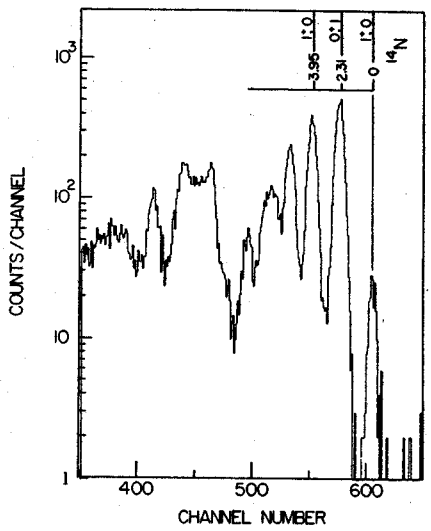

Fig. 1.--Neutron time-of-flight spectrum for $^{14}C(p,n)^{14}N$; Ep=25 MeV, θ_m=60°.